NUMERICAL ANALYSIS OF RECIRCULATING DUCTED FLOWS

R. J. Schulz
ARO, Inc., a Sverdrup Corporation Company

ENGINE TEST FACILITY
ARNOLD ENGINEERING DEVELOPMENT CENTER
AIR FORCE SYSTEMS COMMAND
ARNOLD AIR FORCE STATION, TENNESSEE 37389

December 1978

Final Report for Period October 1, 1977 – February 28, 1978

Prepared for

ARNOLD ENGINEERING DEVELOPMENT CENTER/DOTR
ARNOLD AIR FORCE STATION, TENNESSEE 37389

NOTICES

When U. S. Government drawings, specifications, or other data are used for any purpose other than a definitely related Government procurement operation, the Government thereby incurs no responsibility nor any obligation whatsoever, and the fact that the Government may have formulated, furnished, or in any way supplied the said drawings, specifications, or other data, is not to be regarded by implication or otherwise, or in any manner licensing the holder or any other person or corporation, or conveying any rights or permission to manufacture, use, or sell any patented invention that may in any way be related thereto.

Qualified users may obtain copies of this report from the Defense Documentation Center.

References to named commerical products in this report are not to be considered in any sense as an indorsement of the product by the United States Air Force or the Government.

This report has been reviewed by the Information Office (OI) and is releasable to the National Technical Information Service (NTIS). At NTIS, it will be available to the general public, including foreign nations.

APPROVAL STATEMENT

This report has been reviewed and approved.

Elton R. Thompson

ELTON R. THOMPSON
Project Manager, Research Division
Directorate of Test Engineering

Approved for publication:

FOR THE COMMANDER

Robert W. Crossley

ROBERT W. CROSSLEY, Lt Colonel, USAF
Acting Director of Test Engineering
Deputy for Operations

REPORT DOCUMENTATION PAGE		READ INSTRUCTIONS BEFORE COMPLETING FORM
1 REPORT NUMBER AEDC-TR-78-29	2 GOVT ACCESSION NO.	3 RECIPIENT'S CATALOG NUMBER
4. TITLE (and Subtitle) NUMERICAL ANALYSIS OF RECIRCULATING DUCTED FLOWS		5 TYPE OF REPORT & PERIOD COVERED Final Report - October 1, 1977 - February 28, 1978 6 PERFORMING ORG REPORT NUMBER
7. AUTHOR(s) R. J. Schulz, ARO, Inc., a Sverdrup Corporation Company		8 CONTRACT OR GRANT NUMBER(s)
9 PERFORMING ORGANIZATION NAME AND ADDRESS Arnold Engineering Development Center/DO Air Force Systems Command Arnold Air Force Station, Tennessee 37389		10. PROGRAM ELEMENT, PROJECT, TASK AREA & WORK UNIT NUMBERS Program Element 65807F
11 CONTROLLING OFFICE NAME AND ADDRESS Arnold Engineering Development Center/OIS Air Force Systems Command Arnold Air Force Station, Tennessee 37389		12. REPORT DATE December 1978 13 NUMBER OF PAGES 38
14 MONITORING AGENCY NAME & ADDRESS(if different from Controlling Office)		15. SECURITY CLASS. (of this report) UNCLASSIFIED 15a. DECLASSIFICATION/DOWNGRADING SCHEDULE N/A

16 DISTRIBUTION STATEMENT (of this Report)

Approved for public release; distribution unlimited.

17. DISTRIBUTION STATEMENT (of the abstract entered in Block 20, if different from Report)

18 SUPPLEMENTARY NOTES

Available in DDC

19 KEY WORDS (Continue on reverse side if necessary and identify by block number)

jet mixing flow	experimental data	flow field
gas flow	theory	Navier-Stokes equations
recirculation	subsonic flow	numerical analysis
turbulent mixing	diffusers	
mathematical analysis	flow separation	

20 ABSTRACT (Continue on reverse side if necessary and identify by block number)

A numerical solution procedure for ducted, recirculating flows has been developed and applied to predict both turbulent pipe flow and ducted, coaxial jet mixing with recirculation. The solution procedure is based on a decay-function, finite-difference formulation applied to a system of governing equations based on stream functions and vorticity. The vorticity governing equation is complete in that no source terms have been deleted or neglected in its

DD FORM 1 JAN 73 1473 EDITION OF 1 NOV 65 IS OBSOLETE

20. ABSTRACT (Continued)

derivation from the Navier-Stokes equations. Boundary values for all dependent variables are defined by physically realistic conditions. Solutions obtained indicate that the accuracy of the solution procedure depends on having an accurate turbulent viscosity model.

AFSC
Arnold AFS Tenn

PREFACE

The work reported herein was conducted by the Arnold Engineering Development Center (AEDC), Air Force Systems Command (AFSC), under Program Element 65807F. The results were obtained by ARO. Inc., AEDC Division (a Sverdrup Corporation Company). operating contractor for the AEDC, AFSC, Arnold Air Force Station, Tennessee. The work was done under ARO Project No. E32-POA. Elton R. Thompson was the Air Force project manager. The manuscript was submitted for publication on April 4, 1978.

CONTENTS

ILLUSTRATIONS

Figure Page

APPENDIX

1.0 INTRODUCTION

Subsonic, turbulent, recirculating flow fields exist in ducts where sudden expansions or contractions occur, behind protuberances such as cooling fins and vortex generators, in the diverging sections of wide angled diffusers, within combustors and cavities, and, to some extent, in plenum chambers and test cells of propulsion engine test facilities. Development of the capability to compute this class of flows will greatly enhance the understanding of and design capability for recirculating flow configurations. An important example of this class of flows occurs in the sudden expansion or dump combustors that are used in aircraft and missile propulsion systems. A typical flow configuration is shown in Fig. 1 which illustrates a recirculating flow created by coaxial, two-stream jet mixing. The operation of such combustors depends on the stable, complete burning that occurs in the recirculation zones and eddies that are created by the aerodynamic forces induced by turbulent mixing. Hence, it is important that the flow fields within such combustors be calculated so that efficient, clean operation can be obtained.

Unfortunately, recirculating flows are mathematically described by a coupled set of non-linear or quasi-linear elliptic partial differential equations. The set can contain either the full Navier-Stokes equations, or, can be based on a pair of equations describing the distribution of stream function and vorticity. Solution methods for such equations have been developed during the last two decades based on finite difference techniques. However, few, if any, accurate solutions of the flow field shown in Fig. 1 have been calculated for two primary reasons. First, solution techniques for elliptic flows must be based on iterative procedures. As a result, the calculations must be made with rather crude finite difference meshes to keep the calculation times and computer storage requirements within practical limits. Second, turbulent viscosity models for such flows were not formulated until recently and still remain a topic of research. Other, code-specific problems have been encountered. For example, Schulz (Refs. 1 and 2) using the elliptic recirculating flow solution method provided by Gosman, et al. (Ref. 3), found that predictions of recirculating combustor flows of acceptable appearance could only be obtained after extensive trial and error manipulation of three of the principal variables of the solution procedure: the finite difference mesh configuration used to represent the combustor geometry, the boundary condition for vorticity at the lip of the fuel or oxidizer nozzle, and the constants in the turbulent viscosity model. Three recirculating flows of the type illustrated in Fig. 1 were calculated, and each required a somewhat different combination of the three factors for the best results. Another significant but unresolved problem identified in the studies reported in Refs. 1 and 2 was that the governing equation for vorticity, solved by the code provided in Ref. 3, was incomplete.

Terms involving the derivatives of viscosity arise in the vorticity transport equation when it is derived from the Navier-Stokes equations. Gosman, et al., deleted those terms from the governing equation by assuming that they were negligible compared with all the other terms. However, the effects of these terms on the calculated flow fields have not been determined, and it is probable that they are not negligible.

Because accurate predictions of even the geometrically simple combustor flows, such as Fig. 1, have not been made, a study was undertaken to develop a computer program that can make accurate and practical calculations. In addition, the code was to be based on the complete vorticity transport equation for turbulent flows. To test the accuracy of the code, four turbulent experiments were selected to compare with the theory—an incompressible, fully developed, turbulent pipe flow and three cases of ducted, two-stream jet mixing with recirculation: one constant density, one nonreacting hydrogen-air, and one reacting hydrogen-air.

2.0 THEORY

2.1 METHOD OF ANALYSIS

The method used in the present study to compute field properties of recirculating flows is the method developed by Chien (Ref. 4), which is based on solving a stream function and vorticity formulation of the Navier-Stokes equations for fully elliptic flows. Chein demonstrated the utility of solving the governing systems of equations by a finite difference method using coordinate stretching to provide numerical resolution where required and special "decay functions" to provide numerically stable solutions.

In this investigation, the Navier-Stokes equations were manipulated to form a vorticity transport equation valid for variable-viscosity, variable-density flows. Turbulent transport models and a chemical reaction model were selected. The problem was simplified somewhat by considering that the flows were to occur at constant static pressure, and in fact, the four experimental flows selected for comparison with the theory do occur at nearly constant static pressure.

2.2 DERIVATION OF THE VORTICITY AND STREAM FUNCTION GOVERNING EQUATIONS

The Navier-Stokes equations for two-dimensional steady flow, taken from Ref. 5, are:

$$\rho u \frac{\partial u}{\partial z} + \rho v \frac{\partial u}{\partial r} = -\frac{\partial P}{\partial Z} + \frac{\partial}{\partial Z}\left[\mu\left(2\frac{\partial u}{\partial Z} - \frac{2}{3}\nabla\cdot\vec{v}\right)\right] + \frac{1}{r^{\delta}}\frac{\partial}{\partial r}\left[r^{\delta}\mu\left(\frac{\partial u}{\partial r} + \frac{\partial v}{\partial Z}\right)\right] \quad (1)$$

$$\rho u \frac{\partial v}{\partial Z} + \rho v \frac{\partial v}{\partial r} = -\frac{\partial P}{\partial r} + \frac{\partial}{\partial Z}\left[\mu\left(\frac{\partial u}{\partial r} + \frac{\partial v}{\partial Z}\right)\right]$$

$$+ \frac{1}{r^{\delta}} \frac{\partial}{\partial r}\left[r^{\delta}\mu\left(2\frac{\partial v}{\partial r} - \frac{2}{3}\nabla\cdot\vec{v}\right)\right] - \frac{\mu\delta}{r}\left[\frac{2v}{r} - \frac{2}{3}\nabla\cdot v\right] \qquad (2)$$

where ∇ is the gradient operator, $\vec{v}$ is the total velocity vector, and δ is a parameter such that $\delta = 0$ for plane two-dimensional flows and $\delta = 1$ for two-dimensional flows with axial symmetry. To derive a vorticity transport equation for two-dimensional flows, Eq. (2) was differentiated with respect to Z, Eq. (1) was differentiated with respect to r, and the resulting equations were subtracted one from the other to obtain a single equation which is explicity independent of pressure terms. The definition of vorticity in two-dimensional flows,

$$\Omega = \frac{\partial v}{\partial Z} - \frac{\partial u}{\partial r} \qquad (3)$$

was then introduced, and the single equation remaining from three operations on the Navier-Stokes equation was manipulated into an equation for conservation of vorticity,

$$\frac{\partial^2\Omega}{\partial Z^2} + \frac{\partial^2\Omega}{\partial r^2} - \left(\frac{\rho u}{\mu} - \frac{2}{\mu}\frac{\partial\mu}{\partial Z}\right)\frac{\partial\Omega}{\partial Z} - \left(\frac{\rho v}{\mu} - \frac{2}{\mu}\frac{\partial\mu}{\partial r} - \frac{\delta}{r}\right)\frac{\partial\Omega}{\partial r}$$

$$+ \left[\frac{1}{\mu}\frac{\partial^2\mu}{\partial Z^2} + \frac{1}{\mu}\frac{\partial^2\mu}{\partial r^2} + \delta\left(\frac{\rho v}{\mu r} + \frac{1}{\mu r}\frac{\partial\mu}{\partial r} - \frac{1}{r^2}\right)\right]\Omega$$

$$+ \frac{2}{\mu}\left[\frac{\partial^2\mu}{\partial Z\partial r}\left(\frac{\partial v}{\partial r} - \frac{\partial u}{\partial Z}\right) + \frac{\partial^2\mu}{\partial Z^2}\frac{\partial u}{\partial r} - \frac{\partial^2\mu}{\partial r^2}\frac{\partial v}{\partial Z} + \frac{\partial\mu}{\partial Z}\frac{1}{\partial r}\left(\frac{\partial u}{\partial Z} + \frac{\partial v}{\partial r} + \frac{v\delta}{r}\right)\right.$$

$$\left. - \frac{\partial\mu}{\partial r}\frac{\partial}{\partial Z}\left(\frac{\partial u}{\partial Z} + \frac{\partial v}{\partial r} + \frac{v\delta}{r}\right)\right] + \frac{1}{2\mu}\left[\frac{\partial(u^2 + v^2)}{\partial Z}\frac{\partial\rho}{\partial r} - \frac{\partial(u^2 + v^2)}{\partial r}\frac{\partial\rho}{\partial Z}\right]$$

$$= 0 \qquad (4)$$

In Eq. (4), viscosity is assumed to be a general function for Z and r. In order to apply Eq. (4) to turbulent flows, the only assumption required is that the viscosity (μ) is an "effective" or "eddy" viscosity.

The stream function equation was derived by defining a stream function (ψ) such that

$$d\psi = \rho u r^{\delta}\, dr - \rho v r^{\delta}\, dZ \qquad (5)$$

Then the definition (Eq. (5)) was introducted into Eq. (3), and the result was manipulated to form

$$\frac{\partial^2\psi}{\partial Z^2} + \frac{\partial^2\psi}{\partial r^2} - \frac{\delta}{r}\frac{\partial\psi}{\partial r} - \frac{1}{\rho}\frac{\partial\rho}{\partial Z}\frac{\partial\psi}{\partial Z} - \frac{1}{\rho}\frac{\partial\rho}{\partial r}\frac{\partial\psi}{\partial r} + \rho r^{\delta}\Omega = 0 \tag{6}$$

Equation (6) is the governing equation for the stream function. It is easy to show that the stream function (ψ) automatically and identically satisfied the mass conservation equation for steady flow, i.e..

$$r^{\delta}\frac{\partial}{\partial Z}(\rho u) + \frac{\partial}{\partial r}(\rho v r^{\delta}) = 0 \tag{7}$$

2.3 TURBULENT VISCOSITY MODEL

2.3.1 Constant Viscosity

In this model, the turbulent viscosity is set equal to a selected constant,

$$\mu_t = \mu_{REF} \tag{8}$$

The use of Eq. (8) effectively treats the turbulent flow as a laminar flow.

2.3.2 Algebraically Prescribed Viscosity

Schulz (Ref. 1 and 2) developed the following model to correlate theoretical predictions of recirculating combustor-type flows with experimental data:

$$\mu_t = k_{\mu}\,\rho\, u_j\, R_j\left[1 + Z/(275\,R_j)\right] \tag{9}$$

where k_{μ} is a constant whose value is 0.0285. Equation (9) was developed for two-stream, coaxial jet mixing with recirculation when the duct to jet radius ratio is greater than ten. There is no physical justification for this model except that fully developed, turbulent, free jets can be shown to require a constant viscosity of magnitude ($k_{\mu}\rho u_j R_j$). Numerical experimentation by Schulz showed that, for the recirculating flows of this type, a linearly increasing effective viscosity was required for the best prediction.

2.3.3 Prandtl Mixing Length Viscosity Model

The mixing length model developed by Prandtl is well described by Schlichting (Ref. 6). It has been used to calculate turbulent jets, wakes, boundary layers and pipe flows. In Prandtl's model,

$$\mu_t = \rho\,\ell^2\left|\frac{\partial u}{\partial r}\right| \tag{10}$$

where ℓ is a length scale called the Prandtl mixing length. For fully developed turbulent flow in smooth walled pipes, Schlichting gives

$$\ell = \left[0.14 - 0.08\,(r/R_D)^2 - 0.06\,(r/R_D)^4\right] R_D \tag{11}$$

2.3.4 Turbulent Kinetic Energy-Dissipation Viscosity Model

This model for turbulent viscosity was developed by Spalding and his co-workers and is described by Launder and Spalding (Ref. 7). It has been applied to several types of turbulent flows, including flows with recirculation (Ref. 8) but with only partial success. In this viscosity formulation, the turbulent viscosity is given as

$$\mu_t = C_\mu \rho K^2/\epsilon \tag{12}$$

where C_μ is a constant with the value 0.09. To determine the spatial distribution of K and ϵ in high turbulent Reynolds number flows, two coupled partial differential transport equations must be solved:

$$\frac{\partial}{\partial Z}(\rho u r^\delta K) + \frac{\partial}{\partial r}(\rho v r^\delta K) - \frac{\partial}{\partial Z}\left(\frac{\mu}{\sigma_K} r^\delta \frac{\partial K}{\partial Z}\right) - \frac{\partial}{\partial r}\left(\frac{\mu}{\sigma_K} r^\delta \frac{\partial K}{\partial r}\right) - r^\delta S_K = 0 \tag{13}$$

$$\frac{\partial}{\partial Z}(\rho u r^\delta \epsilon) + \frac{\partial}{\partial r}(\rho v r^\delta \epsilon) - \frac{\partial}{\partial Z}\left(\frac{\mu}{\sigma_\epsilon} r^\delta \frac{\partial \epsilon}{\partial K}\right) - \frac{\partial}{\partial r}\left(\frac{\mu}{\sigma_\epsilon} r^\delta \frac{\partial \epsilon}{\partial r}\right) + r^\delta S_\epsilon = 0 \tag{14}$$

where the parameters σ_K and σ_ϵ are turbulent Schmidt numbers for K and ϵ, respectively, having the values $\sigma_K = 1.0$ and $\sigma_\epsilon = 1.3$.

S_K and S_ϵ are source terms for K and ϵ given by

$$S_K = \rho\epsilon - \mu\left\{2\left[\left(\frac{\partial u}{\partial Z}\right)^2 + \left(\frac{\partial v}{\partial r}\right)^2 + \left(\frac{v\delta}{r}\right)^2\right] + \left(\frac{\partial u}{\partial r} + \frac{\partial v}{\partial Z}\right)^2\right\} \tag{15}$$

$$S_\epsilon = C_{\epsilon_2} \rho \epsilon^2/K - C_{\epsilon_1} \epsilon/K\ \mu\left\{2\left[\left(\frac{\partial u}{\partial Z}\right)^2 - \left(\frac{\partial v}{\partial r}\right) + \left(\frac{v\delta}{r}\right)^2\right] - \left(\frac{\partial u}{\partial r} + \frac{\partial v}{\partial Z}\right)^2\right\} \tag{16}$$

where C_{ϵ_1} and C_{ϵ_2} are constants having the values of 1.45 and 2.0, respectively.

The constant effective viscosity model was used in the evaluation and checkout stage of the program development. The Prandtl mixing length model and the K-ϵ model were used to calculate the turbulent pipe flow, while the algebraic viscosity model was used in the calculation of the jet mixing with recirculation flows.

2.4 EQUATION OF STATE

For incompressible flows, the density was set to an appropriate constant value, but for the nonreactive and reactive calculations, the density at each point in the flow was calculated from the ideal-gas equation of state

$$\bar{\rho} = \frac{\bar{P}\,\bar{W}}{R_G \bar{T}} \tag{17}$$

For the nonreactive calculation, both pressure and temperature were constant, but the molecular weight ($\bar{W}$) had to be calculated at each point in the flow. The molecular weight was computed from the distributions of the mass fractions of hydrogen and air. Once the local value of the mass fraction of air (C) was known, the molecular weight was determined from

$$\bar{W} = 1 \Big/ \left(\frac{C}{28.96} + \frac{1 - C}{2} \right) \tag{18}$$

To determine the spatial distribution of C, a model transport equation, valid for turbulent flows, was solved simultaneously with the governing equations. The equation, obtained from Gosman, et al. (Ref. 3), is

$$\frac{\partial}{\partial Z}\left(\rho u r^{\delta} C\right) - \frac{\partial}{\partial r}\left(\rho v r^{\delta} C\right) - \frac{\partial}{\partial Z}\left(\frac{\mu}{\sigma_C} r^{\delta} \frac{\partial C}{\partial Z}\right) - \frac{\partial}{\partial r}\left(\frac{\mu}{\sigma_C} r^{\delta} \frac{\partial C}{\partial r}\right) = 0 \tag{19}$$

For the reacting flow calculations, the pressure was assumed constant; however, both the temperature and the molecular weight had to be determined at each point of the flow field. To determine their variations, a simplified chemical reaction model and a thin flame sheet model were used. This approach was suggested by Gosman. et al. (Ref. 3). In the present study, the following chemical reaction model for the hydrogen-oxygen-nitrogen system was adopted:

1 Kg Fuel + i Kg Oxidizer + jKg Inert → (i + 1) Kg Products + jKg Inert where for the hydrogen-air reaction, i = 8 and j = 26.3. (20)

The thin flame sheet model was developed to calculate the reaction zone of initially separate fuel and oxidizer streams. It is assumed that the fuel and oxidizer streams are separated by a thin flame sheet such that, on the fuel side of the flame sheet, only the mass fractions of fuel, products, and inert species exist; whereas, on the oxidizer side of the flame sheet, only the mass fractions of oxidizer, products, and inert species exist. The location of the thin flame sheet is the locus of points where the mass fractions of both the fuel and oxidizer have disappeared. To predict the spatial variations of the specie

mass fractions, a transport equation for the chemical reaction parameter C was derived by following the procedure outlined by Gosman, et al. (Ref. 3). The equation is the same as the mass fraction transport equation for the nonreactive flow:

$$\frac{\partial}{\partial Z}(\rho u r^{\delta} C) + \frac{\partial}{\partial r}(\rho v r^{\delta} C) - \frac{\partial}{\partial Z}\left(\frac{\mu}{\sigma_C} r^{\delta} \frac{\partial C}{\partial Z}\right) - \frac{\partial}{\partial r}\left(\frac{\mu}{\sigma_C} r^{\delta} \frac{\partial C}{\partial r}\right) = 0 \qquad (21)$$

but for the reactive flow

$$C = (\tilde{C} - \tilde{C}_{FI})/(\tilde{C}_{\phi I} - \tilde{C}_{FI}) \qquad (22)$$

where FI and ϕI are the fuel and oxidizer inlet conditions, respectively, and

$$\tilde{C} = m_{\varphi} - im_F \qquad (23)$$

The equation for C is solved simultaneously with the governing equations. Once C had been found, locally, the mass fractions of the species were known. Specifically for the hydrogen-air reaction on the fuel side of the flame sheet

$$\begin{aligned} m_I &= 0.7678\,C \\ m_{\varphi} &= 0 \\ m_F &= 1 - 1.029025\,C \\ m_p &= 0.261225\,C \end{aligned} \qquad (24)$$

while on the oxidizer side of the flame sheet

$$\begin{aligned} m_I &= 0.7678\,C \\ m_{\varphi} &= 8.2322\,C - 8 \\ m_F &= 0.0 \\ m_p &= 9(1 - C) \end{aligned} \qquad (25)$$

Thus, the local value of the molecular weight can be determined indirectly as a function of C, since

$$\bar{W} = \left(\frac{m_I}{28} + \frac{m_F}{2} + \frac{m_{\varphi}}{32} + \frac{m_p}{18}\right)^{-1} \qquad (26)$$

To determine the temperature field, the following assumptions were made:

1. The kinetic energy of the mean flow and the turbulence are small compared to the chemical energy of the hydrogen-air reaction.

2. The specific heats of the chemical species are constant.

3. The total enthalpy of the flow which includes both the sensible and chemical energy is everywhere constant. Also the walls of the duct are adiabatic.

By making these assumptions, the static temperature at each point in the flow field is given by

$$\bar{T} = T_{REF} + m_p H_{REF}/(\bar{C}_{p_F} m_F + \bar{C}_{p_I} m_I + \bar{C}_{p_\phi} m + \bar{C}_{p_p} m_p) \quad (27)$$

The reference temperature was assumed to be the static temperature of the inlet hydrogen and air streams which were equal. The reference enthalpy was selected such that the maximum temperature in the flame sheet was the stoichiometric temperature for the hydrogen-air reaction. The values of these parameters were specified as

$$\begin{aligned} T_{REF} &= 294\ ^\circ K \\ H_{REF} &= 12317656.9\ J/Kg \\ \bar{C}_{p_F} &= 16099.0\ J/Kg\text{-}^\circ K \\ \bar{C}_{p_I} &= 1173.9\ J/Kg\text{-}^\circ K \\ \bar{C}_{p_\phi} &= 1048.1\ J/Kg\text{-}^\circ K \\ \bar{C}_{p_p} &= 2431.6\ J/Kg\text{-}^\circ K \end{aligned} \quad (28)$$

For these conditions, the stoichiometric flame temperature for hydrogen and air is

$$T_{STOIC} = 2388.9\ ^\circ K \quad (29)$$

Thus, the density of the reacting hydrogen-air flow was determined (indirectly as a function of C) according to the equation

$$\rho = P \Big/ \left[R_G \left(\frac{m_p}{18} + \frac{m_F}{2} + \frac{m_I}{28} - \frac{m_\Phi}{32} \right) \left(294 + \frac{12317656.9\, m_p}{(1173.9\, m_I + 2431.6\, m_p + 16099\, m_F + 1048.1\, m_\Phi)} \right) \right] \quad (30)$$

2.5 BOUNDARY CONDITIONS

The boundary conditions for the dependent variables were different for the turbulent pipe flow and the jet-mixing flows. The boundary conditions are specified below for both classes of turbulent flow.

2.5.1 Turbulent Pipe Flow

2.5.1.1 Vorticity

Across the inlet of the pipe, the velocity was assumed uniform so that $\Omega = 0$. Along the wall, or rather at the first mesh point off the wall, a slightly modified form of a formula used by Chien (Ref. 4) was adopted,

$$\Omega_{I,JN} = -\Omega_{I,JN-2} + \left(\frac{v_{I+1,JN} - v_{I-1,JN}}{\Delta Z}\right) - \left(\frac{u_{I,JN} - u_{I,JN-2}}{\Delta r}\right) \quad (31)$$

Along the axis of the pipe, $\Omega = 0$, while across the exit of the pipe, the condition $\partial\Omega/\partial Z = 0$ was imposed.

2.5.1.2 Stream Function

For uniform inlet flow, the stream function distribution is $\psi(r) = 1/2\ \rho u r^2$. Along the wall and axis of the pipe, the stream function is constant. At the outlet of the pipe, the condition $\partial\psi/\partial Z = 0$ was imposed.

2.5.1.3 Turbulent Kinetic Energy and Dissipation

Across the inlet of the pipe, K and ϵ were set to a small constant (10^{-6}). Along the wall, the formulas developed by Chien (Ref. 4) were applied, i.e.,

$$K_{JN} = V^{*2}/\sqrt{C_\mu} \quad (32)$$

$$\epsilon_{JN} = \rho_{JN}\ V^{*4}/\mu_{JN} \quad (33)$$

where V* is the local value of the friction velocity defined as $\sqrt{\tau_w/\rho}$. In some calculations, V* was assigned, based on experimental data; whereas in other computations, V* was calculated using the iterative law-of-the-wall matching procedure of Chien (Ref. 4). Across the pipe outlet, the condition $\partial K/\partial Z = \partial\epsilon/\partial Z = 0$ was imposed; while along the axis of the pipe, $\partial K/\partial r = \partial\epsilon/\partial r = 0$.

2.5.2 Ducted Recirculating Flow

2.5.2.1 Vorticity

Across the jet inlet, from the axis to the nozzle lip, the vorticity distribution was assigned by assuming that $\Omega = -\Delta u/\Delta r$. The necessary values for $\Delta u/\Delta r$ were obtained from a 15-point central difference analysis of the velocity profile shown in Fig. 2. This profile was obtained from the smoothed experimental jet profile of Ref. 2. The velocity, vorticity, and stream function distributions were truncated at the radial location $r = R_j - \delta^*$ where δ^* is the displacement thickness of the measured velocity profile. In principle, the truncated part of velocity and velocity profile should have a negligible effect on the downstream flow field, and therefore, it was assumed that it was unnecessary to accurately model this part of the jet exit flow field.

Across the remainder of the inlet plane from jet nozzle lip to the duct wall, along the wall, and along the centerline, the vorticity was set equal to zero. Across the duct outlet plane the condition $\partial\Omega/\partial Z = 0$ was imposed.

2.5.2.2 Stream Function

Across the inlet of the duct, from the axis to the jet nozzle lip, the stream function distribution was obtained by assuming constant jet flow density and numerically integrating the velocity profile (Fig. 2). The integration was carried out such that the relation,

$$u = \frac{1}{\rho r}\frac{\Delta\psi}{\Delta r} \tag{34}$$

would reproduce the velocity profile from the stream function profile. The self-consistency of the velocity and stream-function profiles are indicated in Fig. 2 by the excellent agreement of the calculated velocity with the given profile.

The stream-function distribution over the remainder of the duct inlet from the jet nozzle lip to the wall was determined by assuming constant secondary stream density and velocity, so that

$$\psi(r) = \frac{1}{2}\rho_s u_s(r^2 - R_j^2) + \psi_{\text{JET LIP}} : r \geq R_j \tag{35}$$

Along the wall and along the axis of the duct, the stream-function is constant. Across the outlet of the duct, the condition $\partial\psi/\partial Z = 0$ was imposed.

2.5.2.3 Species Parameter

Across the inlet of the duct, from the axis to the jet nozzle lip, C = 1.0, and from the nozzle lip to the wall, C = 0.0. Along the wall and along the axis, the condition $\partial C/\partial r = 0$ was imposed, while across the outlet plane the condition $\partial C/\partial Z = 0$ was imposed.

3.0 NUMERICAL SOLUTION PROCEDURE

The numerical solution procedure used in the present study was developed and reported by Chien (Refs. 4, 9, and 10). The numerical solution procedure is written in terms of stretched coordinates. Chien used coordinate stretching to transform a physical domain enclosed by diverging diffuser walls into a rectangular computational domain and to provide numerical resolution in the boundary layer. However, in the present study, coordinate stretching is used to stretch the flow field near the central inlet in order to improve the numerical resolution of the solution. The coordinate stretching required in the present study was provided by simple transformation functions of the form

$$\xi = g(Z)$$

$$\eta = f(r) \tag{36}$$

This family includes, for example, power law and logarithmic stretching functions. The transformation factors are

$$\frac{\partial}{\partial Z} = \frac{\partial \xi}{\partial Z}\frac{\partial}{\partial \xi}$$

$$\frac{\partial}{\partial r} = \frac{\partial \eta}{\partial r}\frac{\partial}{\partial \eta}$$

$$\frac{\partial^2}{\partial Z^2} = \frac{\partial^2 \xi}{\partial Z^2}\frac{\partial}{\partial \xi} + \left(\frac{\partial \xi}{\partial Z}\right)^2 \frac{\partial^2}{\partial \xi^2}$$

$$\frac{\partial^2}{\partial r^2} = \frac{\partial^2 \eta}{\partial r^2}\frac{\partial}{\partial \eta} - \left(\frac{\partial \eta}{\partial r}\right)^2 \frac{\partial^2}{\partial \eta^2}$$

$$\frac{\partial^2}{\partial Z \partial r} = \frac{\partial \xi}{\partial Z}\frac{\partial \eta}{\partial r}\frac{\partial^2}{\partial \xi \partial \eta} \tag{37}$$

The coordinate transformations (Eqs. (36) and (37)) were applied to the set of governing partial differential equations, and then each equation of the set was rearranged to the "standard form" proposed by Chien (Ref. 4)

$$a1_\phi \frac{\partial^2 \phi}{\partial \xi^2} - a2_\phi \frac{\partial^2 \phi}{\partial \eta^2} - b1_\phi \frac{\partial \phi}{\partial \xi} - b2_\phi \frac{\partial \phi}{\partial \eta} + d_\phi = 0 \tag{38}$$

The coefficients ($a1_\phi$, $a2_\phi$, $b1_\phi$ and $b2_\phi$) and the source term (d_ϕ) are listed in Appendix A for each of the parameters $\phi = \Omega$, ψ, C, K, and ϵ.

In the "decay function formulation," functions are introduced into the finite difference equations that correspond to the governing equations to make the finite difference equations exact. The decay functions are obtained from local exact solutions of the governing differential equations. If the governing equations are partial differential equations or if the coefficient $a1_\phi$, $a2_\phi$, $b1_\phi$, or $b2_\phi$ vary as functions of coordinate location, then the decay functions provided by Chien's theory are themselves approximate. Interestingly, although all finite difference equations written in analogy to Eq. (38) are cast in central or space centered finite differences, the decay function formulation approaches the classical upwind one-sided difference formulation when the local cell Reynolds number becomes much greater than two.

The local cell Reynolds numbers are defined as

$$R_{\phi_\xi} = b1_\phi \Delta\xi / a1_\phi$$

and

$$R_{\phi_\eta} = b2_\phi \Delta\eta / a2_\phi \tag{39}$$

The decay functions, formulated in the approximate form presented by Chien, are

$$G_{\phi_\xi} = 1 - 0.0625 R^2_{\phi_\xi}; \quad \left|R_{\phi_\xi}\right| \leq 2$$

$$G_{\phi_\xi} = \frac{2}{\left|R_{\phi_\xi}\right|} - \frac{1}{R^2_{\phi_\xi}}; \quad \left|R_{\phi_\xi}\right| > 2 \tag{40}$$

and

$$G_{\phi_\eta} = 1 - 0.0625 R^2_{\phi_\eta}; \quad \left|R_{\phi_\eta}\right| \leq 2$$

$$G_{\phi_\eta} = \frac{2}{\left|R_{\phi_\eta}\right|} - \frac{1}{R^2_{\phi_\eta}}; \quad \left|R_{\phi_\eta}\right| > 2$$

Each governing equation is written in the space-centered finite difference form

$$\frac{{}^{a1}\phi}{{}^{G}\phi_{\xi}}\left[\left(\frac{\phi_{I+1,J}+\phi_{I-1,J}-2\phi_{IJ}}{\Delta\xi^2}\right)-\left(\frac{{}^{R}\phi_{\xi}\,{}^{G}\phi_{\xi}}{\Delta\xi}\right)\left(\frac{\phi_{I-1,J}-\phi_{I-1,J}}{2\Delta\xi}\right)\right]$$

$$+\frac{{}^{a2}\phi}{{}^{G}\phi_{\eta}}\left[\left(\frac{\phi_{I,J-1}+\phi_{I,J-1}-2\phi_{IJ}}{\Delta\eta^2}\right)-\left(\frac{{}^{R}\phi_{\eta}\,{}^{G}\phi_{\eta}}{\Delta\eta}\right)\left(\frac{\phi_{I,J-1}-\phi_{I,J-1}}{2\Delta\eta}\right)\right]$$

$$+d_{\phi_{I,J}}=0 \tag{41}$$

This equation is solved algebraically for $\phi_{I,J}$ which results in the equation

$$\phi_{I,J}=C_{\phi_{I+1}}\phi_{I+1,J}+C_{\phi_{I-1}}\phi_{I-1,J}+C_{\phi_{J+1}}\phi_{I,J+1}+C_{\phi_{J-1}}\phi_{I,J-1}+D_{\phi_{I,J}} \tag{42}$$

where the coefficients are

$$C_{\phi_{I+1}}=\left[a1_{\phi}/\Delta\xi^2\,G_{\phi_{\xi}}-b1_{\phi}/2\Delta\xi\right]\Big/C_{R_{\phi}}$$

$$C_{\phi_{I-1}}=\left[a1_{\phi}/\Delta\xi^2\,G_{\phi_{\xi}}-b1_{\phi}/2\Delta\xi\right]\Big/C_{R_{\phi}}$$

$$C_{\phi_{J+1}}=\left[a2_{\phi}/\Delta\eta^2\,G_{\phi_{\eta}}-b2_{\phi}/2\Delta\eta\right]\Big/C_{R_{\phi}}$$

$$C_{\phi_{J-1}}=\left[a2_{\phi}/\Delta\eta^2\,G_{\phi_{\eta}}+b2_{\phi}/2\Delta\eta\right]\Big/C_{R_{\phi}}$$

$$C_{R_{\phi}}=2\left[a1_{\phi}/\Delta\xi^2\,G_{\phi_{\xi}}-a2_{\phi}/\Delta\eta^2\,G_{\phi_{\eta}}\right] \tag{43}$$

and the source term is

$$D_{\phi_{IJ}}=d_{\phi_{I,J}}/C_{R_{\phi}} \tag{44}$$

Equation (42) was used as a successive substitution formula for $\phi_{I,J}$. An iterative field point subroutine was developed to obtain convergent solution for each variable (Ω, ψ, C, K, and ϵ) in a point-by-point manner. The rate of convergence was controlled by an appropriate relaxation factor.

4.0 COMPARISON OF THEORY AND EXPERIMENT

4.1 TURBULENT PIPE FLOW

The numerical algorithm was checked by using the constant effective viscosity model to predict fully developed laminar pipe flow. The predictions agreed exactly with the known analytic solution (Ref. 6). Then a series of calculations was made of a turbulent pipe flow investigated and reported by Laufer (Ref. 11). Distributions of axial velocity and turbulent kinetic energy across the flow in a smooth-walled pipe were derived from Laufer's data for a Reynolds number of 500,000, which served as the basis for comparison with the theory.

The first calculation was made by using the experimental data to establish the boundary conditions for velocity and friction velocity. The boundary conditions were applied at the radial location $\bar{r} = 0.05$ because the viscosity models are not valid in the laminar sublayer which lies next to the wall. The Prandtl mixing length viscosity model was applied to make this calculation. Comparison of theory and experiment is shown in Fig. 3. The velocity field is excellently predicted but the turbulent kinetic energy distribution near the wall is lower than experiment. The next calculation was made by applying a law-of-the-wall matching procedure used by Chien (Ref. 4) for assigning values of velocity outside the laminar sublayer. In this procedure, the friction velocity and the axial velocity at the boundary point ($\bar{r} = 0.05$) are obtained during the course of the solution by using the velocity at the second point from the wall ($\bar{r} = 0.105$) in the law-of-the-wall relationship

$$\frac{u}{V^*} = 2.5 \log_e (V^* y/\nu) + 5.5 \tag{45}$$

to solve for V^*. Then, the velocity at the boundary point is calculated from Eq. 45. The results of this calculation are shown in Fig. 4. Again, the axial velocity distribution is well predicted, but the turbulent kinetic energy distribution falls below the experiment. Thus, the boundary value for K is too small, since with $C_\mu = 0.09$

$$K_{JN} = V^{*2}/\sqrt{0.09} = 3.33V^{*2} \tag{46}$$

hence, as shown in Fig. 4, $0.2\ K/V^{*2} = 0.67$ at the matching point, $\bar{r} = 0.05$. But the experimental data imply that $0.2\ K_w/V^{*2} = 0.9$ which requires that $C_\mu = 0.05$ at the wall. So, as Chien (Ref. 4) and others have pointed out, C_μ must vary across the turbulent pipe flow, tending to about 0.05 at the boundary point. Therefore, for the following calculations, C_μ was allowed to vary linearly from 0.09, at the radial location $\bar{r} = 0.25$, to 0.05 at the wall, $\bar{r} = 0$. Both the Prandtl mixing length viscosity model and the

K-ϵ viscosity model were used to calculate the flow by applying the law-of-the-wall matching procedure. The results are shown in Fig. 5. Both models provided good predictions of the axial velocity distributions, although the Prandtl mixing length model does best, and both models predicted about the same turbulent kinetic energy distributions which are in good agreement with the experimental data. Also, both models predicted the wall friction velocity to within three percent.

The Reynolds number for all the calculations was 5.2×10^5 based on the pipe diameter; the calculations with a 20 by 20 uniform mesh took less than five minutes using an IBM 370/165 computer.

4.2 DUCTED, TWO-STREAM, COAXIAL JET MIXING WITH RECIRCULATION

4.2.1 Constant Density Jet Mixing

An experiment reported by Barchilon and Curtet (Ref. 12) was selected as a test case for this type flow. The data reported were taken in an experimental configuration similar to that shown in Fig. 1. To make calculations of this flow, the algebraic viscosity model (Eq. (9)) was applied together with the boundary conditions described in Section 2.5.2. It should be noted that the experimental data were obtained in a water tunnel where the jet velocity was about 12.8 m/sec, and the duct-to-jet radius ratio was 13.33. In the calculations, the fluid is air, the jet velocity is 205.7 m/sec, and the duct-to-jet radius ratio is 10. However, both flows have the same Craya-Curtet number and, therefore, should be similar according to theory (Ref. 13).

Figure 6 shows a comparison between experimental and theoretical distributions of axial velocity on the centerline of the duct. While the theoretical predictions appear to decay at the proper rate, the length of the potential core of the central jet is not well predicted. Moreover, the predicted velocity slightly overshoots the inlet or boundary value for jet velocity. On the other hand, the distributions of axial velocity across the duct are in reasonably good agreement with the experiment, as shown in Fig. 7.

As was stated in the Introduction, one objective of the present investigation was to determine whether the vorticity source terms that have been neglected in previous recirculating flow calculations (e.g., Refs. 1, 2, 3, and 8) are significant. For the constant density jet calculations, numerical experiments were performed by repeating the calculation of the Barchilon and Curtet experiment but without the terms

$$S_\Omega = \frac{2}{\mu}\left[\frac{\partial^2\mu}{\partial Z\partial r}\left(\frac{\partial v}{\partial r}-\frac{\partial u}{\partial Z}\right)+\frac{\partial^2\mu}{\partial Z^2}\frac{\partial u}{\partial r}-\frac{\partial^2\mu}{\partial r^2}\frac{\partial v}{\partial Z}+\frac{\partial\mu}{\partial Z}\frac{\partial}{\partial r}\left(\frac{\partial u}{\partial Z}+\frac{\partial v}{\partial r}+\frac{v\delta}{r}\right)\right.$$

$$\left.-\frac{\partial\mu}{\partial r}\frac{\partial}{\partial Z}\left(\frac{\partial u}{\partial Z}+\frac{\partial v}{\partial r}+\frac{v\delta}{r}\right)\right] \quad (47)$$

in the vorticity source term in Eq. (4). The calculated velocity field is also shown in Figs. 6 and 7 where the results are nearly indistinguishable. Thus, for constant-density flows with slowly varying eddy viscosity, i.e., for nearly laminar incompressible flows, the vorticity source terms (Eq. (47)) may be neglected.

These calculations required about five minutes using a 20 by 50 mesh. The mesh was uniform in the radial direction and slightly stretched in the axial direction.

4.2.2 Variable-Density, Nonreactive Jet Mixing

An experiment reported by Schulz (Refs. 1 and 2) of ducted, coaxial, two-stream variable-density jet mixing was selected as a test case. The flow field corresponds to that shown in Fig. 1. The variable-density flow was isothermal, and the density variations were due to the molecular weight difference between the central and annular streams. The mixing in this experiment occurred between a central air jet and a surrounding stream of hydrogen in which the air jet inlet velocity was about 206 m/sec. The ratio of the duct radius to the jet radius was 10.

The algebraic viscosity model (Eq. (9)) was again used together with the same mesh and boundary conditions used to calculate the constant density case. The complete vorticity source term was included in the vorticity transport equation. Equation (19) was solved for the mass fraction of air. Figure 8 shows a comparison of experimental and theoretical distributions of hydrogen mass fraction along the centerline and the wall of the duct and the distribution of axial velocity along the centerline of the duct. The predicted velocity distribution is in satisfactory agreement with the experiment. But, the predicted hydrogen mass fractions show greater diffusion and spreading than experiment. Also the predicted fully mixed mass fraction is eight percent higher than experiment. On the other hand, the predicted axial velocity distributions across the duct are in good agreement with the data (Fig. 9). The hydrogen mass fraction distributions at the corresponding axial positions are compared with data in Fig. 10, which also shows that the predicted hydrogen mass fraction field has greater spreading and diffusion than the experiment indicates. Thus, it would appear that, for the variable-density flow, a better turbulent viscosity model is required.

The effect of deleting the viscosity-dependent vorticity source terms (Eq. (47)) in the variable-density calculation is also shown in Figs. 8 and 9. Figure 8 shows that by deleting the terms (Eq. (47)) significant velocity overshoot occurs in the near field. Thus, for this specific flow, these terms have a significant effect on the predicted flow field. On the other hand, comparison of the axial velocity distributions across the duct shows that the terms have a relatively unimportant effect on the shapes of the far field velocity

profiles. Therefore, the complete vorticity source term should be incorporated in variable density calculations because of their effect on the near field.

Other numerical experimentation showed that the inlet plane distribution of viscosity can also affect the calculated flow field one mesh line downstream because it enters the calculation through the viscosity-dependent terms of Eq. (47). Thus, by including the full vorticity source term in the calculation procedure, all of the inlet plane boundary values must be consistently described, and this, in a sense, forces the solution procedure to be physically realistic. Calculation time for this case was approximately 20 min on the IBM 370/165.

4.2.3 Variable-Density, Reacting Jet Mixing

A real combustor flow field is characterized by regions wherein large heat release rates from the burning gases cause both molecular weight and temperature gradients. So that, in turbulent reacting flow, the time-averaged density depends on the time-averaged temperature and the time-averaged molecular weight. The process can be represented either as

$$\bar{\rho} = \overline{(P\bar{W}/R_G T)} \tag{48}$$

or as

$$\bar{\rho} = \bar{P}\,\bar{w}/R_G\,\bar{T} \tag{49}$$

In the present study, the latter definition has been adopted, as explained in Section 2.4. The approach was applied to calculate the reacting, recirculating combustor flow reported by Chriss (Ref. 14). The data obtained by Chriss were taken in the configuration shown in Fig. 1. The mixing and chemical reaction was between a central air stream and a surrounding hydrogen stream having the same velocity and radius ratios as those of the previously discussed nonreactive case.

Theoretical predictions were made without changing the mesh, the inlet or boundary conditions, or the viscosity model from those applied in the nonreactive flows. The equation for the species parameter (Eq. (21)) was added to the set of governing equations. The theoretical predictions are compared with experiment in Figs. 11, 12, and 13. While the hydrogen at any point of the flow may be contained in either water vapor or atomic or molecular hydrogen, the experimental data do not enable the distribution of the hydrogen among the molecular species to be determined. Thus, the hydrogen mass fractions indicated in the figures is the total or atomic mass fraction. Also, as shown in

Figs. 11 and 12, there are two velocity curves marked "experimental." One velocity curve represents velocity measured by laser velocimetry. The other "experimental" velocity curves were calculated from the measured pitot and static pressures and the hydrogen atom mass fraction by assuming that chemical equilibrium existed at each point in the flow field.

The predicted velocity distribution along the centerline of the duct shows a very large overshoot, which, however, falls between the two "experimental" curves. This makes it difficult to determine whether the chemistry or the turbulent viscosity model is in error. Another, more significant problem is that the theoretically predicted axial distributions of hydrogen mass fraction exceeds the experiment in the far field by 75 percent. Thus, the numerical solutions are not preserving the species mass, probably because of the large overshoot of the velocity field. In order to resolve the problem, numerical experimentation would be required beyond the scope of the present study. The axial velocity profiles across the flow at three axial stations are compared with experiment in Fig. 12. They are not as well predicted as the nonreactive case showing greater spreading than the experimental data. The hydrogen mass fraction profiles across the duct are compared with experiment in Fig. 13. The shapes of the calculated hydrogen atom fraction profiles are fairly well predicted, although the magnitudes are significantly different. Thus, the reacting, recirculating flow has not been satisfactorily predicted. Although the chemistry model used in the present study is undeniably crude, the computational experience gained in this study implies that the principal effort in the future should be to develop a turbulence transport model that will accurately predict the near field of the jet mixing process in this class of recirculating flows. The calculation time for this flow field was about 40 min.

5.0 CONCLUDING REMARKS

The calculation procedure for recirculating combustor flows, based on solving a system of equations for vorticity, stream function, and species parameter by using the decay-function, finite-difference scheme of Chien, has been evaluated by comparisons with four sets of experimental data - turbulent pipe flow, and three recirculating flows. The turbulent pipe flow (Laufer) and the case of constant density recirculating flow (Barchilon and Curtet) were predicted with acceptable accuracy. The axial velocity field of the nonreacting, variable-density recirculating flow (Schulz) was acceptably well predicted, but the predicted species mass fraction field showed too great of a rate of diffusion and spreading. In this calculation, the species were conserved to within eight percent of the experimental results in the far field. Neither the axial velocity field nor the species field of the reacting, variable-density combustor flow (Chriss) were well predicted. The theoretical calculations showed a large velocity overshoot, but it could not

be determined whether the viscosity model or the chemistry model caused this effect. The far field species concentration was 75 percent greater than experiment, indicating that, for this case, the solution did not conserve species.

It was shown that, for variable-density recirculating flows. the vorticity source term should be complete because the terms that have been considered negligible in other studies have a significant effect on the quality of the solution in the near field. Also, it was found that because of the retained source terms, the inlet boundary values of velocity, density, and viscosity must be consistent because they affect the numerical solution downstream by interaction with the source terms in the vorticity equations.

The primary research goal in the future studies should be to develop turbulent viscosity models that are applicable to the strong, developing shear layers that exist in the recirculating flows of the type studied herein. Until an adequate viscosity model is obtained, it is probably not worthwhile considering more complex chemistry models for these flows.

REFERENCES

1. Schulz, R. J. "An Investigation of Ducted, Two-Stream, Variable Density, Turbulent Jet Mixing with Recirculation." AEDC-TR-76-152 (ADA034537), AFOSR-TR-76-1087, January 1977.

2. Schulz, R. J. "An Experimental and Theoretical Investigation of Confined, Two-Stream Variable Density, Turbulent Jet Mixing with Recirculation." Ph.D. Dissertation, The University of Tennessee, Knoxville, 1976.

3. Gosman, A. D., Pun, W. K., Ruchal, A. K., Spalding, B. D., and Wolfshtein, M. Heat and Mass Transfer in Recirculating Flows. Academic Press, New York, 1969.

4. Chien, J. C. "Numerical Analysis of Turbulent Separated Subsonic Diffuser Flows." AEDC-TR-76-159 (ADA036005), February 1977.

5. Bird, R. B.. Stewart, W. E., and Lightfoot, E. N. Transport Phenomena. John Wiley and Sons, Inc., New York, 1960.

6. Schlichting, H. Boundary Layer Theory. Sixth Edition, McGraw-Hill Book Company, Inc., New York, 1966.

7. Launder, B. E., and Spalding, D. B. Lectures on Mathematical Models of Turbulence. Academic Press, Inc., New York, 1972.

8. Elghobashi, S. E. "Characteristics of Gaseous Turbulent Diffusion Flames in Cylindrical Chambers." Ph.D. Dissertation, Mechanical Engineering Department, Imperial College of Science and Technology, London, England, 1974.

9. Chien, J. C. "A General Finite-Difference Formulation with Application to Navier-Stokes Equations." Journal of Computational Physics, Vol. 20, Number 3, March 1976, pp. 268-278.

10. Chien, J. C. "A General Finite-Difference Formulation with Application to Navier-Stokes Equations." Computers and Fluids, Vol. 5, 1977, pp. 15-31.

11. Laufer. J. "The Structure of Turbulence in Fully Developed Pipe Flow." NACA Report 1174, 1954.

12. Barchilon, M. and Curtet, R. "Some Details of the Structure of an Axisymmetric Confined Jet with Backflow." Transactions of the ASME Journal of Basic Engineering, Vol. 86, December 1964, pp. 777-787.

13. Becker, H. A., Hottle, H. C., and Williams, G. C. "Mixing and Flow in Ducted Turbulent Jets." Proceedings of the Ninth Symposium (International) on Combustion, Academic Press. Inc., Vol. I, New York, 1963, pp. 7-20.

14. Chriss, D. E. "An Experimental Investigation of Ducted, Reactive, Turbulent Jet Mixing with Recirculation." AEDC-TR-77-56 (ADA044110), AFOSR-TR-77-0749, September 1977.

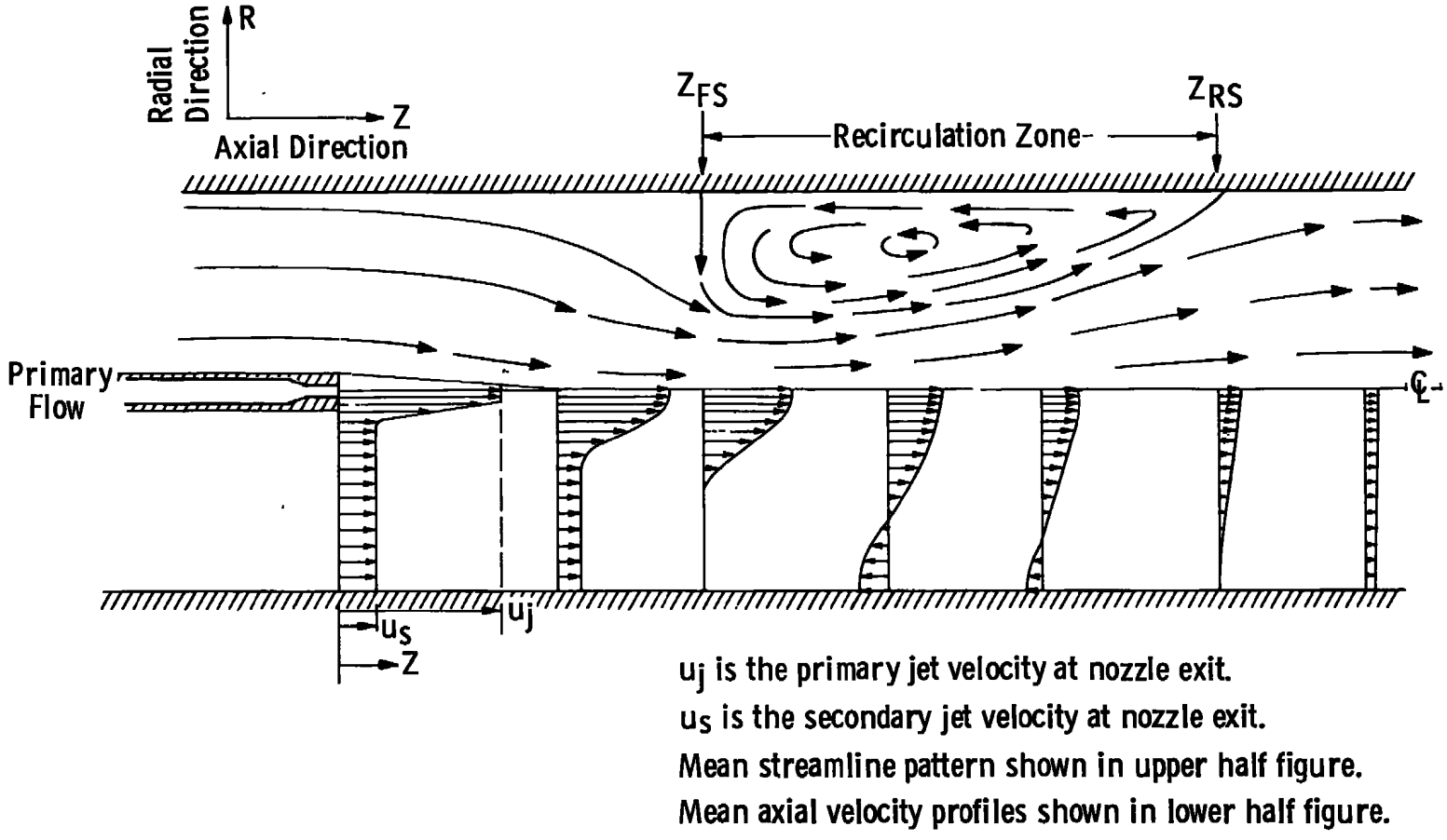

Figure 1. Turbulent, ducted, mixing system with recirculation.

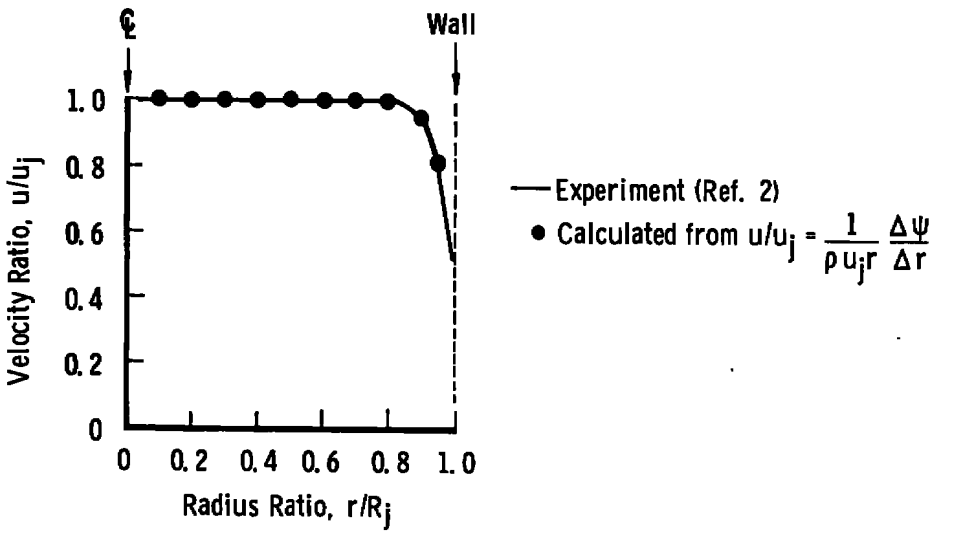

Figure 2. Velocity profile across central jet nozzle used to define u, Ω, and ψ distributions for the ducted jet-mixing calculations.

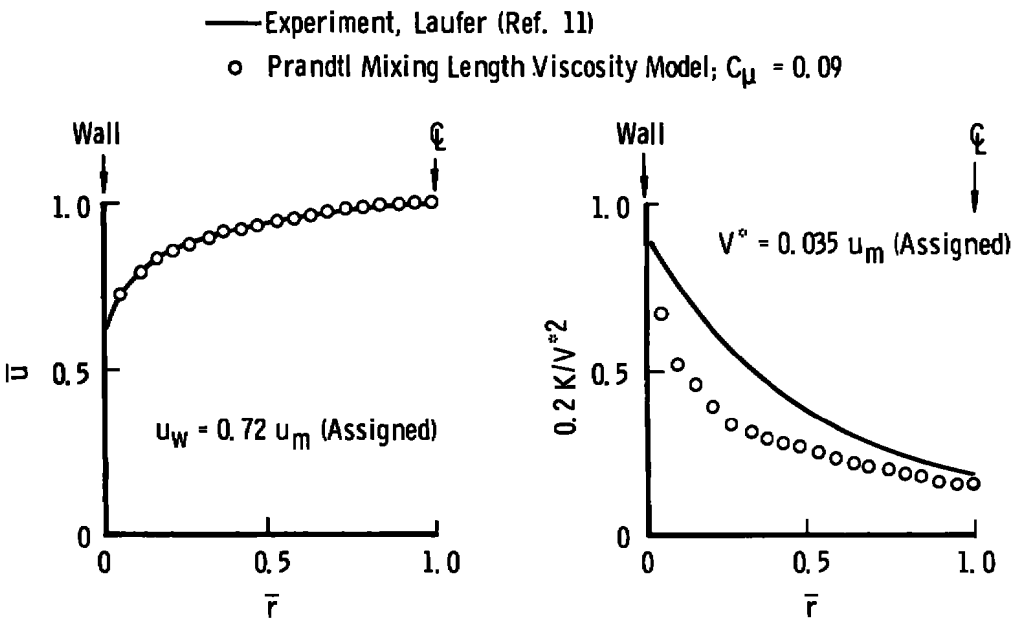

Figure 3. Comparison of experimental and theoretical distributions of axial velocity and turbulent kinetic energy across a turbulent pipe flow.

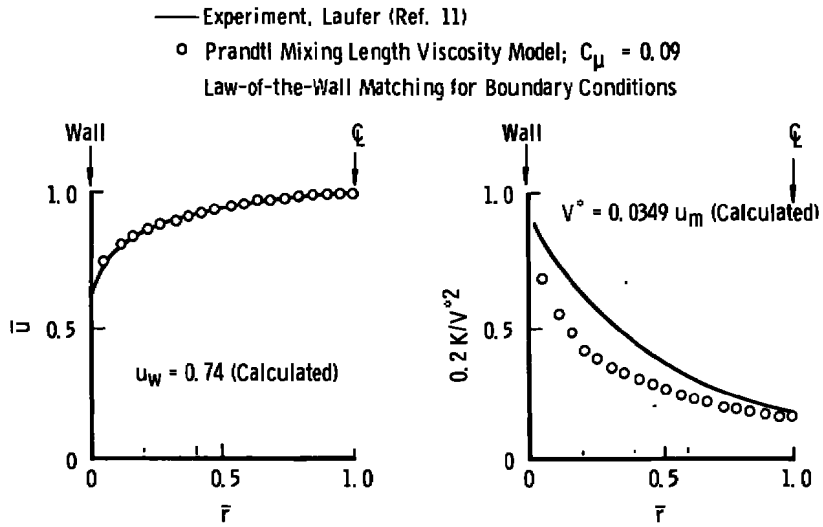

Figure 4. Comparison of experimental and theoretical distributions of axial velocity and turbulent kinetic energy across a turbulent pipe flow with law-of-the-wall matching.

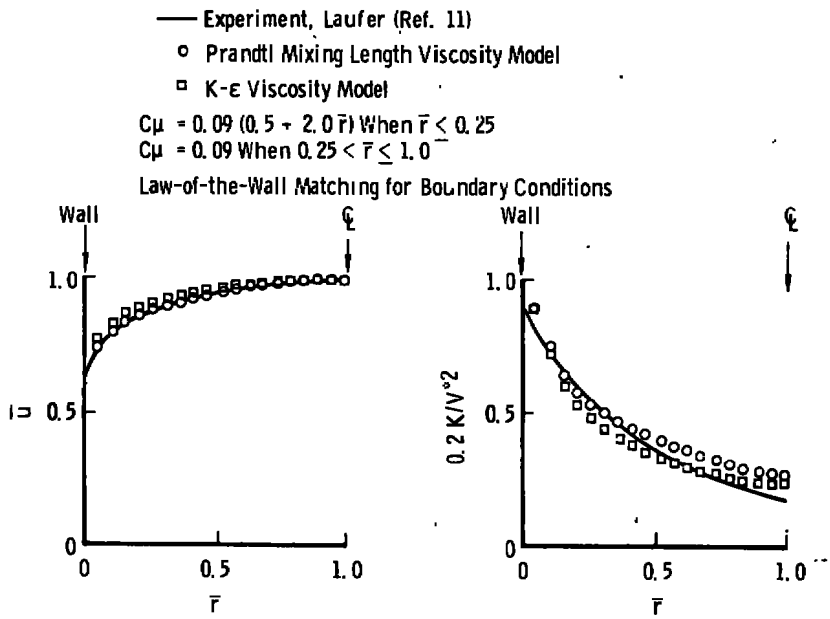

Figure 5. Comparison of experimental and theoretical distributions of axial velocity and turbulent kinetic energy across a turbulent pipe flow with K-ε viscosity model.

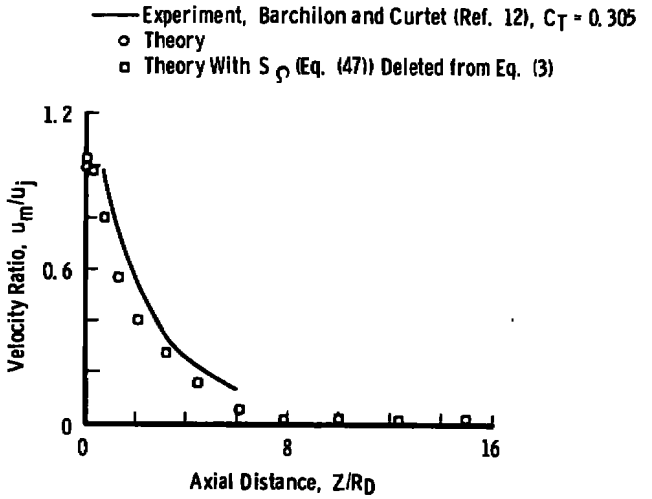

Figure 6. Comparison of experimental and theoretical distributions of axial velocity on the centerline for constant-density, ducted jet mixing.

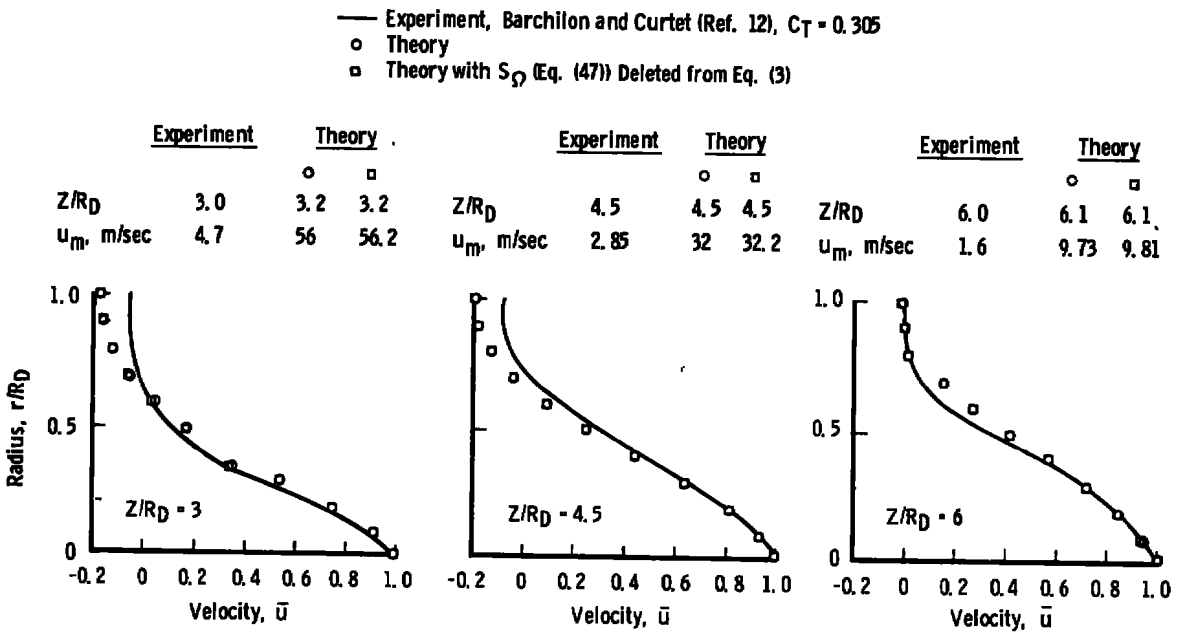

Figure 7. Comparison of experimental and theoretical velocity distributions at three axial locations for constant-density, ducted jet mixing.

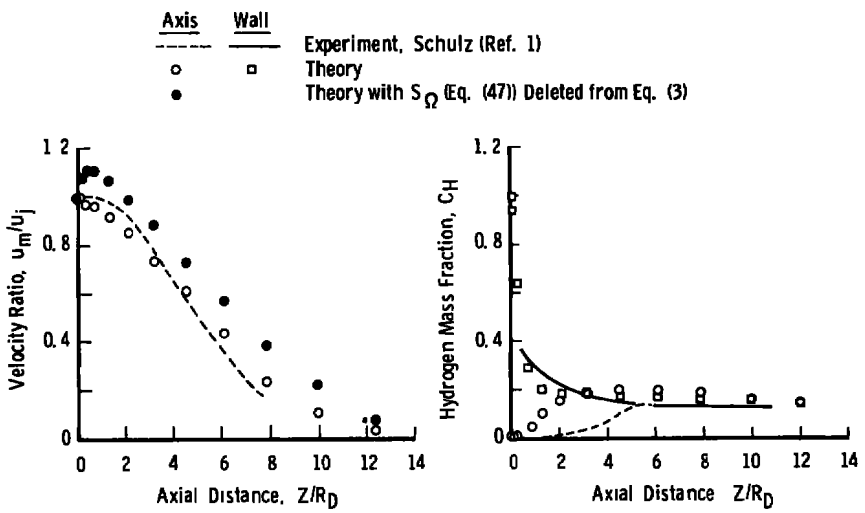

Figure 8. Comparison of experimental and theoretical distributions of axial velocity and hydrogen mass fraction for variable-density, ducted jet mixing.

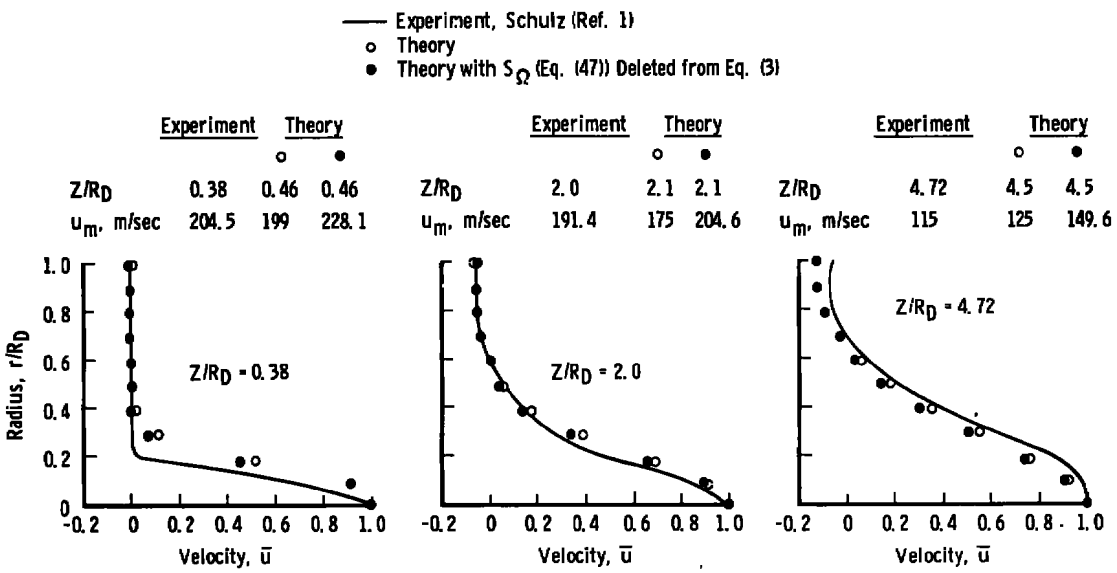

Figure 9. Comparison of experimental and theoretical velocity distributions at three axial locations for variable-density, ducted jet mixing.

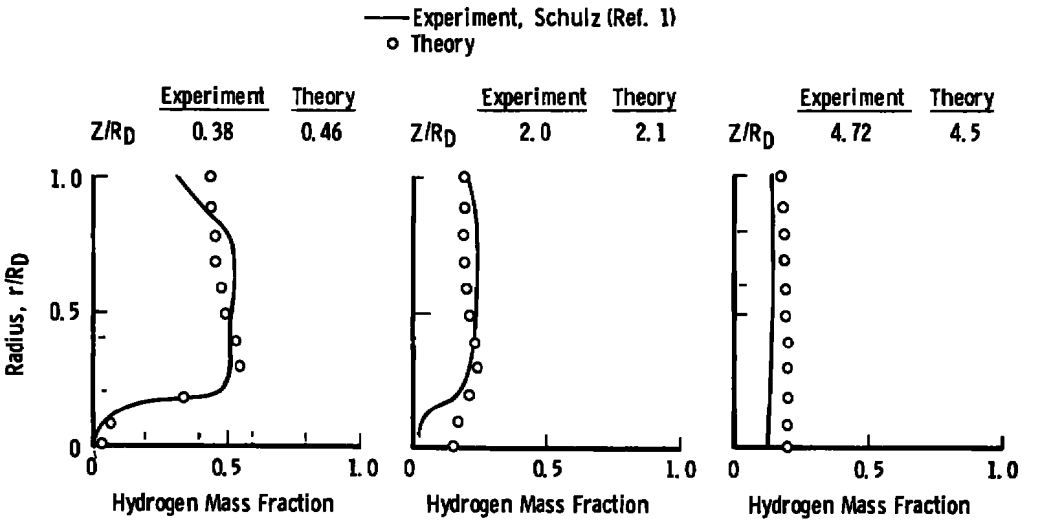

Figure 10. Comparison of experimental and theoretical distributions of hydrogen mass fraction at three axial locations for variable-density, ducted jet mixing.

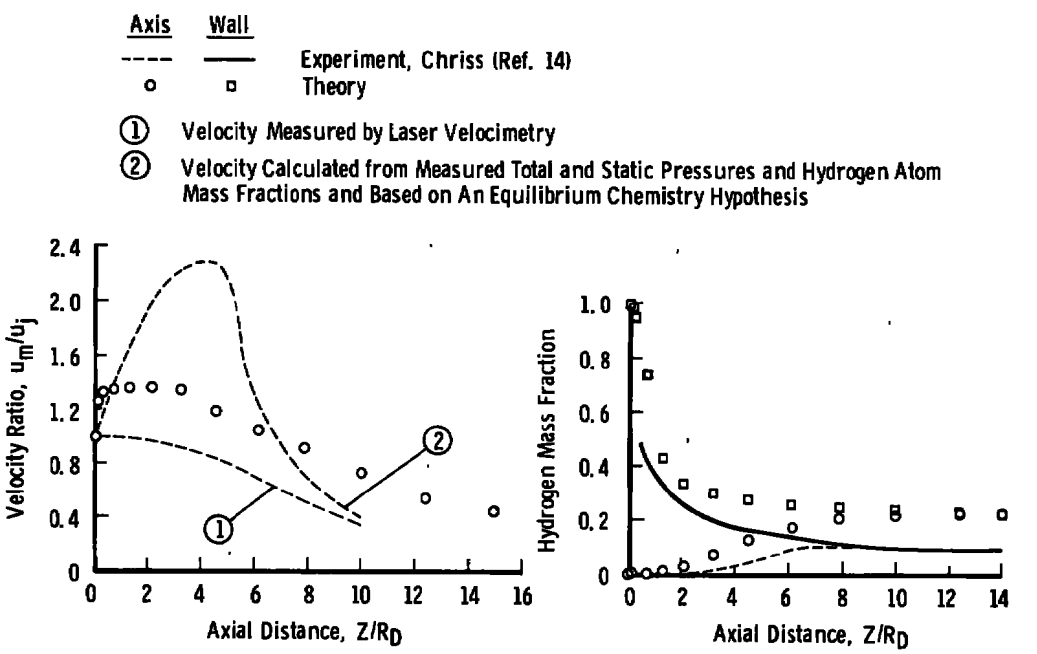

Figure 11. Comparison of experimental and theoretical distributions of axial velocity and hydrogen mass fractions for variable-density, reacting jet mixing.

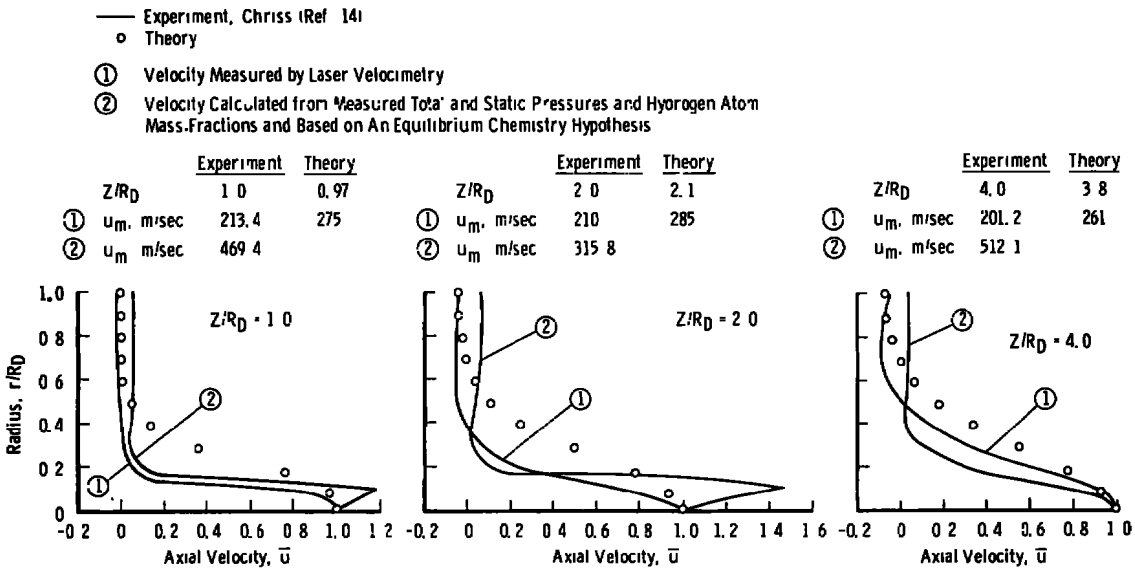

Figure 12. Comparison of experimental and theoretical velocity distributions at three axial locations for variable-density, reacting jet mixing.

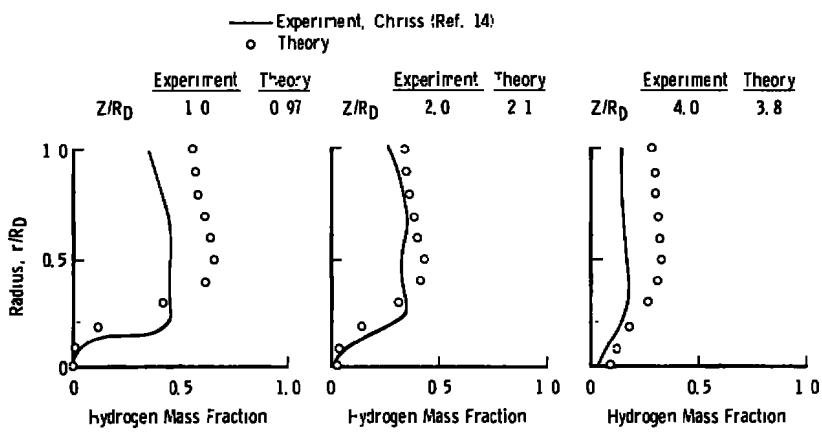

Figure 13. Comparisons of experimental and theoretical distributions of hydrogen atom mass fractions at three axial locations for variable-density, reacting jet mixing.

APPENDIX A
COEFFICIENTS IN THE STANDARD FORM OF THE GOVERNING EQUATION

I. Vorticity

$$a1_{\Omega} = \left(\frac{\partial \xi}{\partial Z}\right)^2$$

$$a2_{\Omega} = \left(\frac{\partial \eta}{\partial r}\right)^2$$

$$b1_{\Omega} = \left[\left(\frac{\rho u}{\mu} - \frac{2}{\mu}\frac{\partial \xi}{\partial Z}\frac{\partial \mu}{\partial \xi}\right)\frac{\partial \xi}{\partial Z} - \frac{\partial^2 \xi}{\partial Z^2}\right]$$

$$b2_{\Omega} = \left[\left(\frac{\rho v}{\mu} - \frac{2}{\mu}\frac{\partial \eta}{\partial r}\frac{\partial \mu}{\partial \eta} - \frac{\delta}{r}\right)\frac{\partial \eta}{\partial r} - \frac{\partial^2 \eta}{\partial r^2}\right]$$

$$d_{\Omega} = \left\{\frac{1}{\mu}\left[\left(\frac{\partial \xi}{\partial Z}\right)^2 \frac{\partial^2 \mu}{\partial \xi^2} + \frac{\partial^2 \xi}{\partial Z^2}\frac{\partial \mu}{\partial \xi} - \left(\frac{\partial \eta}{\partial r}\right)^2 \frac{\partial^2 \mu}{\partial \eta^2}\right.\right.$$

$$\left. + \frac{\partial^2 \eta}{\partial r^2}\frac{\partial \mu}{\partial \eta}\right] + \delta\left[\frac{\rho v}{\mu r} + \frac{1}{\mu r}\frac{\partial \mu}{\partial \eta}\frac{\partial \eta}{\partial r} - \frac{1}{r^2}\right]\Bigg\} \Omega$$

$$+ \frac{2}{\mu}\left\{\left[\frac{\partial \xi}{\partial Z}\frac{\partial \eta}{\partial r}\frac{\partial^2 \mu}{\partial \xi \partial \eta}\left(\frac{\partial \eta}{\partial r}\frac{\partial v}{\partial \eta} - \frac{\partial \xi}{\partial Z}\frac{\partial u}{\partial \xi}\right)\right] + \left[\left(\frac{\partial \xi}{\partial Z}\right)^2 \frac{\partial^2 \mu}{\partial \xi^2} + \frac{\partial^2 \xi}{\partial Z^2}\frac{\partial \mu}{\partial \xi}\right]\frac{\partial \eta}{\partial r}\frac{\partial u}{\partial \eta}\right.$$

$$- \left[\left(\frac{\partial \eta}{\partial r}\right)^2 \frac{\partial^2 \mu}{\partial \eta^2} + \frac{\partial^2 \eta}{\partial r^2}\frac{\partial \mu}{\partial \eta}\right]\frac{\partial \xi}{\partial Z}\frac{\partial v}{\partial \xi}$$

$$+ \frac{\partial \xi}{\partial Z}\frac{\partial \mu}{\partial \xi}\left[\frac{\partial \xi}{\partial Z}\frac{\partial \eta}{\partial r}\frac{\partial^2 u}{\partial \xi \partial \eta} + \frac{\partial^2 \eta}{\partial r^2}\frac{\partial v}{\partial \eta} + \left(\frac{\partial \eta}{\partial r}\right)^2 \frac{\partial^2 v}{\partial \eta^2}\right.$$

$$+ \frac{\delta}{r}\frac{\partial \eta}{\partial r}\frac{\partial v}{\partial \eta} - \frac{v\delta}{r^2}\Bigg] - \frac{\partial \eta}{\partial r}\frac{\partial \mu}{\partial \eta}\left[\frac{\partial^2 \xi}{\partial Z^2}\frac{\partial u}{\partial \xi}\right.$$

$$\left.\left. + \left(\frac{\partial \xi}{\partial Z}\right)^2 \frac{\partial^2 u}{\partial \xi^2} + \frac{\partial \xi}{\partial Z}\frac{\partial \eta}{\partial r}\frac{\partial^2 v}{\partial \xi \partial \eta} + \frac{\delta}{r}\frac{\partial \xi}{\partial Z}\frac{\partial v}{\partial \xi}\right]\right\}$$

$$+ \frac{1}{\mu}\left[\frac{\partial \xi}{\partial Z}\frac{\partial}{\partial \xi}\left(\frac{u^2+v^2}{2}\right)\frac{\partial \eta}{\partial r}\frac{\partial \rho}{\partial \eta} - \frac{\partial \eta}{\partial r}\frac{\partial}{\partial \eta}\left(\frac{u^2+v^2}{2}\right)\frac{\partial \xi}{\partial Z}\frac{\partial \rho}{\partial \xi}\right]$$

II. Stream Function

$$a1_{\psi} = \left(\frac{\partial \xi}{\partial Z}\right)^2$$

$$a2_{\psi} = \left(\frac{\partial \eta}{\partial r}\right)^2$$

$$b1_{\psi} = \left(\frac{1}{\rho}\frac{\partial \xi}{\partial Z}\frac{\partial \rho}{\partial \xi} - \frac{\partial^2 \xi}{\partial Z^2}\right)$$

$$b2_{\psi} = \left(\frac{1}{\rho}\frac{\partial \eta}{\partial r}\frac{\partial \rho}{\partial \eta} + \frac{\delta}{r}\frac{\partial \eta}{\partial r} - \frac{\partial^2 \eta}{\partial r^2}\right)$$

$$d_{\psi} = \rho r^{\delta}\Omega$$

III. Species Parameter,

$$a1_C = \left(\frac{\partial \xi}{\partial Z}\right)^2$$

$$a2_C = \left(\frac{\partial \eta}{\partial r}\right)^2$$

$$b1_C = \left[\left(\frac{\rho u \sigma_C}{\mu} - \frac{1}{\mu}\frac{\partial \xi}{\partial Z}\frac{\partial \mu}{\partial \xi}\right)\frac{\partial \xi}{\partial Z} - \frac{\partial^2 \xi}{\partial Z^2}\right]$$

$$b2_C = \left[\left(\frac{\rho v \sigma_C}{\mu} - \frac{1}{\mu}\frac{\partial \eta}{\partial r}\frac{\partial \mu}{\partial \eta} - \frac{\delta}{r}\right)\frac{\partial \eta}{\partial r} - \frac{\partial^2 \eta}{\partial r^2}\right]$$

$$d_C = 0$$

IV. Turbulent Kinetic Energy

$$a1_K = \left(\frac{\partial \xi}{\partial Z}\right)^2$$

$$a2_K = \left(\frac{\partial \eta}{\partial r}\right)^2$$

$$b1_K = \left[\left(\frac{\rho u \sigma_K}{\mu} - \frac{1}{\mu}\frac{\partial \xi}{\partial Z}\frac{\partial \mu}{\partial \xi}\right)\frac{\partial \xi}{\partial Z} - \frac{\partial^2 \xi}{\partial Z^2}\right]$$

$$b2_K = \left[\left(\frac{\rho v \sigma_K}{\mu} - \frac{1}{\mu}\frac{\partial \eta}{\partial r}\frac{\partial \mu}{\partial \eta} - \frac{\delta}{r}\right)\frac{\partial \eta}{\partial r} - \frac{\partial^2 \eta}{\partial r^2}\right]$$

$$d_K = -\rho\epsilon + \mu\left\{2\left[\left(\frac{\partial \xi}{\partial Z}\frac{\partial u}{\partial \xi}\right)^2 + \left(\frac{\partial \eta}{\partial r}\frac{\partial v}{\partial \eta}\right)^2 + \left(\frac{v\delta}{r}\right)^2\right] - \left(\frac{\partial \eta}{\partial r}\frac{\partial u}{\partial \eta} + \frac{\partial \xi}{\partial Z}\frac{\partial v}{\partial \xi}\right)^2\right\}$$

V. Dissipation

$$a1_\epsilon = \left(\frac{\partial \xi}{\partial Z}\right)^2$$

$$a2_\epsilon = \left(\frac{\partial \eta}{\partial r}\right)^2$$

$$b1_\epsilon = \left[\left(\frac{\rho u \sigma_\epsilon}{\mu} - \frac{1}{\mu}\frac{\partial \xi}{\partial Z}\frac{\partial \mu}{\partial \xi}\right)\frac{\partial \xi}{\partial Z} - \frac{\partial^2 \xi}{\partial Z^2}\right]$$

$$b2_\epsilon = \left[\left(\frac{\rho v \sigma_\epsilon}{\mu} - \frac{1}{\mu}\frac{\partial \eta}{\partial r}\frac{\partial \mu}{\partial \eta} - \frac{\delta}{r}\right)\frac{\partial \eta}{\partial r} - \frac{\partial^2 \eta}{\partial r^2}\right]$$

$$d_\epsilon = -C_{K_2}\rho\frac{\epsilon^2}{K} + C_{K_1}\frac{\epsilon}{K}\mu\left\{2\left[\left(\frac{\partial \xi}{\partial Z}\frac{\partial u}{\partial \xi}\right)^2 + \left(\frac{\partial \eta}{\partial r}\frac{\partial v}{\partial \eta}\right)^2 + \left(\frac{v\delta}{r}\right)^2\right] + \left(\frac{\partial \eta}{\partial r}\frac{\partial u}{\partial \eta} + \frac{\partial \xi}{\partial Z}\frac{\partial v}{\partial \xi}\right)^2\right\}$$

NOMENCLATURE

$a1_\phi$, $a2_\phi$	Coefficients in the standard form of the governing equations, Eq. (38)
$b1_\phi$, $b2_\phi$	Coefficients in the standard form of the governing equations, Eq. (38)
C	Species parameter, either mass fraction of air, or given by Eq. (22)
$\tilde{C}$	Species parameter, Eq. (23)
C_p	Specific heat at constant pressure
C_T	Craya-Curtet Number, Ref. 1
d_ϕ, D_ϕ	Source term for the dependent variable
G_ϕ	Decay function for the dependent variable ϕ, Eq. 40
H_{REF}	Reference enthalpy
I	Mesh index for axial position
J	Mesh index for radial position
K	Turbulent kinetic energy per unit mass
ℓ	Prandtl Mixing Length, Eq. (11)
m_F, m_φ, m_P, m_I	Mass fractions of fuel, oxidizer, product and inert species, respectively
P	Static pressure
r	Radial coordinate
$\bar{r}$	Nondimensional radial coordinate, $(R_D - r)/R_D$, zero at the wall
R_D	Duct radius
R_G	Universal gas constant
R_j	Jet radius
$\bar{T}$	Static temperature

u	Axial velocity
$\bar{u}$	Nondimensional axial velocity, $\bar{u} = u/u_m$
u_j	Jet velocity
u_m	Maximum axial velocity at a given axial position
u_s	Secondary stream velocity
u_w	Wall velocity at $\bar{r} = 0.05$
V^*	Friction velocity, $V^* = \sqrt{\tau_w/\rho}$
v	Radial velocity
$\overline{W}$	Molecular weight, Eqs. (18) or (26)
Z	Axial coordinate
δ^*	Boundary layer displacement thickness
ϵ	Dissipation rate of turbulent kinetic energy
ξ	Stretched axial coordinate
η	Stretched radial coordinate
μ	Dynamic viscosity, $\mu = \mu_t + \mu_L$
μ_t	Turbulent viscosity
μ_L	Laminar viscosity
ν	Kinematic viscosity, $\nu = \mu_L/\rho$
ρ	Density
ψ	Stream function, Eq. (5)
ϕ	Dependent variable, either Ω, ψ, C, K, or ϵ
τ_w	Wall shear stress
Ω	Vorticity, Eq. (3)

SUBSCRIPT

FS	Forward stagnation point
JN	Radial matching point outside the laminar sublayer in pipe flow
RS	Rear stagnation point
ξ	With respect to stretched axial coordinate
η	With respect to stretched radial coordinate

SUPERSCRIPT

$-$	An over bar represents a time-averaged quantity